Catalytic Features of the Botulinum Neurotoxin A Light Chain Revealed by High Resolution Structure of an Inhibitory Peptide Complex[†,‡]

Nicholas R. Silvaggi,[§] David Wilson,[||] Saul Tzipori,[⊥] and Karen N. Allen*[,§]

Department of Physiology and Biophysics, Boston University School of Medicine, Boston, Massachusetts 02118, Center for Neurologic Diseases, Brigham and Women's Hospital and Department of Neurology, Harvard Medical School, Cambridge, Massachusetts 02139, and Division of Infectious Diseases, Tufts University School of Veterinary Medicine, North Grafton, Massachusetts 01536

Received January 19, 2008; Revised Manuscript Received April 8, 2008

ABSTRACT: The *Clostridium botulinum* neurotoxin serotype A light chain (BoNT/A-LC) is a Zn(II)-dependent metalloprotease that blocks the release of acetylcholine at the neuromuscular junction by cleaving SNAP-25, one of the SNARE proteins required for exocytosis. Because of the potential for use of the toxin in bioterrorism and the increasingly widespread application of the toxin in the medical field, there is significant interest in the development of small-molecule inhibitors of the metalloprotease. Efforts to design such inhibitors have not benefited from knowledge of how peptides bind to the active site since the enzyme−peptide structures available previously either were not occupied in the vicinity of the catalytic Zn(II) ion or did not represent the product of SNAP-25 substrate cleavage. Herein we report the 1.4 Å-resolution X-ray crystal structure of a complex between the BoNT/A-LC and the inhibitory peptide N-Ac-CRATKML, the first structure of the light chain with an inhibitory peptide bound at the catalytic Zn(II) ion. The peptide is bound with the Cys Sγ atom coordinating the metal ion. Surprisingly, the cysteine sulfur is oxidized to the sulfenic acid form. Given the unstable nature of this species in solution, is it likely that oxidation occurs on the enzyme. In addition to the peptide-bound structure, we report two structures of the unliganded light chain with and without the Zn(II) cofactor bound at 1.25 and 1.20 Å resolution, respectively. The two structures are nearly identical, confirming that the Zn(II) ion plays a purely catalytic role. Additionally, the structure of the Zn(II)-bound uncomplexed enzyme allows identification of the catalytic water molecule and a second water molecule that occupies the same position as the peptidic oxygen in the tetrahedral intermediate. This observation suggests that the enzyme active site is prearranged to stabilize the tetrahedral intermediate of the protease reaction.

The anaerobic, spore-forming bacterium *Clostridium botulinum* produces the most potent toxins known: the botulinum neurotoxins (BoNT) (*1*). The toxins, of which there are seven serotypes (A−G), block the release of acetylcholine at the neuromuscular junction by proteolysis of soluble *N*-ethylmaleimide-sensitive factor attachment protein receptor (SNARE[1]) proteins required for exocytosis. Serotypes A, C, and E cleave synaptosome-associated protein of 25 kDa (SNAP-25), each at a single, unique peptide bond; the serotype C toxin also cleaves syntaxin. Serotypes B, D, F, and G all cleave the vesicle-associated membrane protein (VAMP). The extreme potency of the *Clostridium botulinum* neurotoxins and the ease with which they can be produced and distributed makes these protein toxins a potential bioterrorism threat (*2–5*). In addition, in recent years, BoNTs have become popular agents for the treatment of a rising number of neuromuscular and cosmetic conditions (*6–10*). The persistence of intoxication by serotype A toxin makes it the most useful and potentially hazardous of the seven serotypes. The widespread use of BoNTs, particularly BoNT/A in the medical field, and the need for biodefense measures necessitate the development of small-molecule drugs to modulate or reverse BoNT intoxication.

BoNTs are produced as a single 150 kDa polypeptide chain that is subsequently cleaved by endogenous proteases to give the dichain holotoxin. The holotoxin comprises a heavy chain (HC, ∼100 kDa) and a light chain (LC, ∼50 kDa) linked by a disulfide bond (*11, 12*). The HC contains a C-terminal domain that targets the holotoxin to the presynaptic membrane of motor neurons and triggers internalization by endocytosis (*13–15*) and an N-terminal domain responsible for translocation of the LC from the endosome into the

[†] Financial support comes principally from the Offices of Biological and Environmental Research and of Basic Energy Sciences of the US Department of Energy, and from the National Center for Research Resources of the National Institutes of Health. This work was supported by contract NO1-AI30050 from the National Institutes of Health and the National Institute of Allergy and Infectious Diseases, and NIH training grant HL07291 (to N.R.S.).

[‡] The coordinates and structure factors of BoNT/A light chain in the apo form and complexed with Zn(II) and Zn(II) plus the inhibitory peptide N-Ac-CRATKML have been submitted to the PDB with accession codes 3BOK, 3BON, and 3BOO, respectively.

* To whom correspondence should be addressed. Karen N. Allen, 715 Albany Street R-702, Boston, MA 02118. Tel: 617-638-4398. Fax: 617-638-4273. E-mail: drkallen@bu.edu.

[§] Boston University School of Medicine.

[||] Harvard Medical School.

[⊥] Tufts University School of Veterinary Medicine.

[1] Abbreviations: SNARE, soluble *N*-ethylmaleimide-sensitive factor attachment protein receptor; SNAP-25, synaptosome-associated protein of 25 kDa; VAMP, vesicle-associated membrane protein; BoNT/A-LC, Botulinum neurotoxin serotype A light chain.

10.1021/bi8001067 CCC: $40.75
Published on Web 05/06/2008

cytosol (*16–18*). The toxicity of BoNTs is due to the action of the LC, a Zn(II)-dependent endoprotease that, in the case of the serotype A toxin (BoNT/A), cleaves the Gln197-Arg198 peptide bond of SNAP-25 (Figure 1A). The BoNT LCs are remarkable among proteases for the extremely long substrates required for efficient proteolysis. With a minimum substrate of 17 amino acids (SNKTRIDQANQRATKML, cleavage site underlined), the BoNT/A protease accepts shorter peptide substrates than any of the other serotypes. In comparison, other microbial metalloproteases have been found to have activity against substrates as short as dipeptides (*19*). Structural and biochemical data (*20, 21*) on the BoNT/A-LC suggest that most of the specific interactions between the enzyme and the SNAP-25 substrate occur at sites remote from the active site, termed the α and β exosites (*20*). Indeed, the only amino acid within the cleavage sequence that is required for efficient proteolysis is the P1′ Arg198.

Some of the most informative results have come from X-ray crystal structures of BoNT LCs in enzyme−substrate complexes: the structure of the BoNT/B-LC with synaptrobrevin bound (*22*) and the BoNT/A-LC complexed with SNAP-25 (*20, 23*). Both structures provide important information about the enzyme exosites and the ways in which the LCs interact with their SNARE protein substrates. Additionally, the structures of the serotype A (*18*) and B (*24*) holotoxins provide a further source of information about how Clostridial neurotoxins bind peptide substrates. One outstanding feature of these holotoxin structures is the so-called belt regions of the translocation domains (residues 492−545 in BoNT/A) that wrap around the LC in a manner remarkably similar to that observed in the BoNT/A-LC complex with SNAP-25. It has been proposed that the belt regions constitute surrogate psuedosubstrate inhibitors of their respective LCs (*25*). Thus, a consensus is building concerning the requirement of BoNTs for long substrates and the strategies that these enzymes use to bind extended peptides. However, the apparent lack of specific interactions between the substrate and the enzyme active site presents significant obstacles in the rational design of small-molecule inhibitors.

More than 15 years of research has yielded several potent inhibitors of the BoNT/A-LC (*26–29*), including a number of hydroxamic acid compounds and cysteine-containing peptides. Extensive work on the substrate specificity and mechanism of the BoNT/A-LC (*21, 30–34*) led to the design of a cysteine-based heptapeptide inhibitor, *N*-acetyl-CRATKML-amide, derived from residues 197−203 of SNAP-25 ($K_i = 1.9$ μM) (*35*). Subsequent structure/activity studies on a variant peptide, mpp-RATKML ($K_i = 0.3$ μM) (*36*), intended to probe the contributions of each of the seven residues, showed that with the exception of the P1′ arginine, the BoNT/A-LC active site is not specific for particular amino acid residues. Nonetheless, because a seven-residue peptide is not long enough to simultaneously occupy both the active site and either exosite, it is clear that binding of these short, competitive inhibitors relies on specific interactions in the enzyme active site. More information is needed in order to determine how peptide ligands interact with the catalytic center.

Structural information about the modes of binding of peptides should aid efforts to design potent small-molecule inhibitors. The structures described herein represent the first insight into how inhibitory peptides bind to the BoNT/A metalloprotease active site.

EXPERIMENTAL PROCEDURES

Crystallization and Data Collection. Purified BoNT/A-LC (residues 1−425) was obtained from Dr. L. Smith of the United States Army Medical Research Institute for Infectious Diseases (USAMRIID) as a frozen stock (−80 °C) at 1 mg/mL in solution with 50 mM $NaPO_4$ (pH 6.0) and 2 mM EDTA. The protein was thawed at 4 °C and concentrated to 6−8 mg/mL in preparation for crystallization. Initial crystallization conditions were identified using the PEG/Ion Screen (Hampton Research). Optimization of the most promising condition from the screen, 20% polyethylene glycol (PEG) 3,350, 0.2 M diammonium tartrate (pH 6.6) did not improve the size, quality, or reproducibility of the crystals. Thus, crystals were grown by the hanging-drop vapor diffusion method against reservoirs containing 500 μL of the original PEG/Ion Screen solution. Crystals grew either as aggregates of thick, interconnected plates or large, single, rectangular prisms (ca. 0.5 × 0.3 × 0.2 mm) in two to three days at room temperature (22−23 °C).

It is noteworthy that the large, rectangular prisms diffracted X-rays quite poorly in comparison to even small pieces of the plate-shaped crystals. The diffraction limit for the large crystals was 2.2−2.7 Å, while the smaller plates diffracted to better than 1.1 Å. Not surprisingly, the unit-cell dimensions are also different for the two crystal forms. The poorly diffracting prisms belong to space group $P2_12_12$ ($a = 57.8$; $b = 192.3$; and $c = 40.0$ Å) with two molecules per asymmetric unit. The plate-shaped crystals, in contrast, belong to space group $P2_1$ ($a = 50.1$; $b = 66.6$; $c = 65.4$ Å) with one molecule per asymmetric unit. Because of their superior diffraction, all data were collected from the plate-shaped crystal form.

Single plates were mechanically separated from aggregates using a fine wire probe. The crystal used to determine the apo-LC structure was transferred directly to paratone N and flash-cooled in a gaseous N_2 stream at 100 K. The crystals used to determine the uncomplexed LC and LC·CRATKML structures were soaked prior to cryo-cooling in the crystallization solution plus 10 mM $Zn(NO_3)_2$ for 4.5 h or 5 mM $Zn(NO_3)_2$ and 2 mM N-Ac-CRATKML (GenScript Corp, Piscataway, NJ, USA) for 23 h, respectively. X-ray diffraction data were collected at the National Synchrotron Light Source, Brookhaven National Laboratory, Beamline X12B. Data were processed with DENZO and SCALEPACK (*37*). Data collection and processing statistics are provided in Table 1.

Structure Determination and Model Refinement. The structure of apo-LC was determined by molecular replacement in PHASER (*38*) using the published uncomplexed structure of BoNT/A-LC (residues 1−424 (LC[424]), pdb ID 2IMC) (*39*) as the search model. The model was refined in PHENIX (subroutine phenix.refine) (*40*) with the maximum likelihood target. Ordered solvent molecules were added automatically in phenix.refine and culled manually in the graphics program COOT (*41*). Sections of the model not present in the original LC[424] structure (e.g., the 200 and 250 loops) were built in COOT and refined in phenix.refine. Hydrogen atoms were added to the model in phenix.reduce

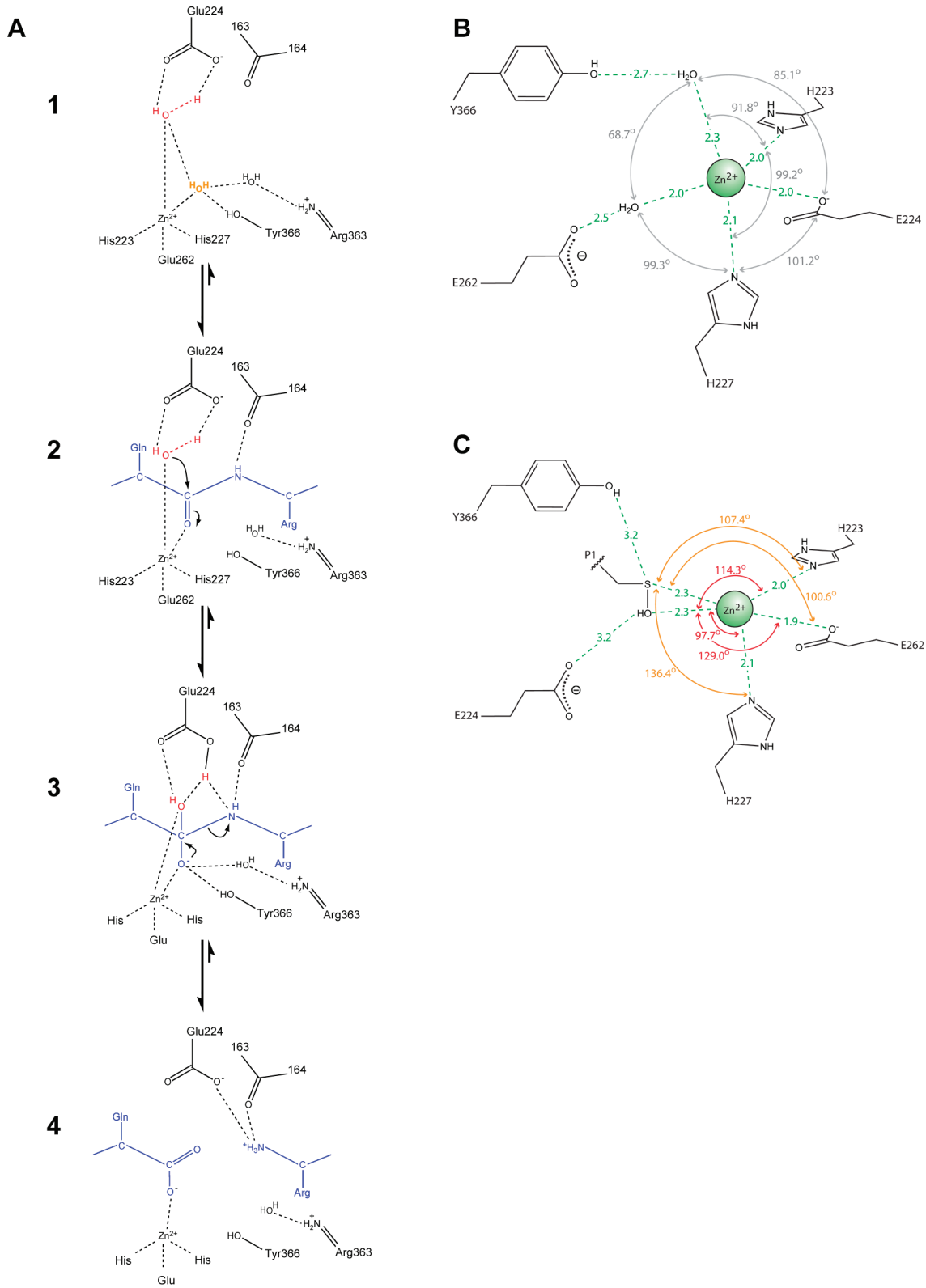

FIGURE 1: Schematic of a proposed BoNT/A-LC mechanism based on the high-resolution uncomplexed LC structure (A) showing the coordination of the Zn(II) ion in the unliganded enzyme (panel 1). W^{Cat} and W^{Tyr} are colored red and orange, respectively. This proposed mechanism is very similar to that proposed for thermolysin (*59*) and for BoNT/A (*55*). Schematic of the Zn(II) coordination spheres in the uncomplexed LC (B) and LC·CRATKML (C) structures. The angles for the various interactions are shown with gray arcs. Binding of N-Ac-CRATKML alters the coordination sphere of the Zn(II) ion to distorted tetrahedral geometry. It cannot be determined from this structure alone whether the CysP1 Sγ or Oδ (or both) provides the fourth Zn ligand. The angles for tetrahedral geometry with Sγ and Oδ acting as ligands are shown with orange and red arcs, respectively. These images were created using ChemDraw Ultra (CambridgeSoft, Inc.) and Adobe Illustrator (Adobe, Inc.).

and were included in the later stages of refinement to improve the stereochemistry of the model. Positions of H atoms were refined using the riding model with a global B-factor. Once the apo-LC refinement converged ($R = 0.129$, $R_{free} = 0.165$),

Table 1: Crystallographic Data Collection and Refinement Statistics

	LC·CRATKML	uncomplexed LC	apo LC
Data Collection			
space group	$P2_1$	$P2_1$	$P2_1$
unit cell dimensions			
a, *b*, *c* (Å)	50.1, 66.6, 65.4	49.5, 66.6, 65.4	49.5, 66.4, 65.1
β (°)	98.7	99.4	99.5
resolution (Å)[a]	50.0 − 1.40 (1.45 − 1.40)	50.0 − 1.20 (1.24 − 1.20)	50.0 − 1.25 (1.29 − 1.25)
R_{symm}	0.055 (0.341)	0.048 (0.286)	0.065 (0.273)
$I/\sigma I$	20.5 (2.6)	16.2 (2.3)	22.3 (3.2)
completeness	95.5 (79.6)	95.8 (87.0)	94.8 (67.4)
redundancy	3.5 (3.1)	3.5 (2.8)	3.5 (2.4)
Model Refinement			
resolution (Å)	21.0 − 1.40	19.7 − 1.20	24.44 − 1.24
no. of reflections	79,759	125,605	109,623
R_{work}/R_{free}	0.149/0.178	0.132/0.161	0.129/0.165
no. of non-H atoms			
protein	3,846	3,886	3,761
ligands/ions	61	1	NA
solvent	613	674	789
ave. B factors (Å^2)			
protein	21.8	14.1	15.9
ligands/ions	23.2	8.9	NA
solvent	32.2	26.8	33.3
rms deviations			
bond lengths (Å)	0.010	0.010	0.015
bond angles (deg)	1.067	1.082	1.205
estimated coordinate error (Å)[b]	0.15	0.13	0.14

[a] The values in parenthesis relate to the highest-resolution shell. [b] Calculated by PHENIX.refine using the formula described in ref *58*.

the model was used to determine the uncomplexed LC and LC·CRATKML structures by the difference Fourier method. All three structures were refined using the same protocol. The heptapeptide inhibitor was not added to the model until the protein and solvent models were nearly complete. Since the electron density for the first four residues was extremely well defined, these were added to the model first. After several rounds of refinement, the electron density for the last three residues of the peptide improved, and these were consequently added to the model. The final models were validated using tools implemented in COOT and MOLPROBITY (*42*). Refinement statistics and model geometry for all three structures are listed in Table 1.

RESULTS AND DISCUSSION

High-Resolution Uncomplexed LC Structure. Uncovering the interactions that BoNT/A-LC makes with its metal cofactor and peptidic substrates in the metalloprotease active site is critical to the understanding of the complete catalytic mechanism and to guide future design of therapeutic inhibitors. Herein, we have approached this problem by determining the structures of the unliganded apo and Zn(II) bound BoNT/A-LC, as well as the Zn(II)-bound complex of the enzyme with a small, peptidic inhibitor. The BoNT/A-LC construct utilized throughout this study is truncated ((residues 1−425; LC[425]; 13 C-terminal amino acids removed) but otherwise wild type in sequence and conformation, as shown previously by comparison with the structure of the full-length LC in the holotoxin complex (*39*).

The structures of the BoNT/A-LC in both the apo (apo LC) and Zn(II)-bound (uncomplexed LC) forms represent the highest-resolution structural information available for the BoNT/A-LC. The increased resolution provides more accurate atomic positions and allows the refinement of individual anisotropic displacement parameters, yielding information about the magnitude and direction of thermal motion of atoms in the model. Comparison of the apo- and uncomplexed LC[425] models to known uncomplexed LC models (3BTA (*18*), 2IMC (*39*), 1XTF (*20*), 2ISE (*43*), 2ISG (*43*), 2ISH (*43*), and 2G7K (*44*)) indicates that the new models do not differ significantly from those determined previously (rmsd for Cα atoms of 0.63−0.99 Å). The apo LC structure confirms that the role of the Zn(II) ion is exclusively catalytic and not structural (*44*). Not only is the apo LC structure globally identical to the uncomplexed structures, but there are no significant local rearrangements of active site residues when the Zn(II) ion is absent.

The number of waters bound to the catalytic Zn(II) ion varies in the previously determined structures of unliganded BoNT/A-LC (2ISE, 2ISG, and 2ISH (*43*)). In structure 2ISH, only one water is observed bound to the Zn(II) ion, while in 2ISG, there are two water molecules within hydrogen bond distance of the Zn(II). In the high-resolution (1.2 Å) uncomplexed LC structure, the catalytic Zn(II) ion is pentacoordinate with ligands provided by His223, His227, Glu262, and two ordered water molecules held in place by Glu224 (W^{Cat}) and Tyr366 (W^{Tyr}) (Figure 1B). W^{Cat} and W^{Tyr} are 2.4 Å apart, and their positions overlay exactly with those in the previously determined structures 2ISH and 2ISG. A similar situation occurs in the related Zn(II)-dependent metalloprotease thermolysin (*45*). Thus, there are two distinct solvent-binding sites at the catalytic center. The fact that W^{Cat} is present more often than W^{Tyr} suggests that the W^{Cat}-binding site has higher affinity for solvent. It would seem, then, that W^{Tyr} highlights the position of an oxyanion binding site, an assertion supported by the observation that the two oxygen atoms in a model of the Gln-Arg tetrahedral transition state (data not shown) overlay exactly with W^{Cat} and W^{Tyr}. This observation, in turn, suggests that the enzyme active site is prearranged to stabilize the tetrahedral intermediate of the

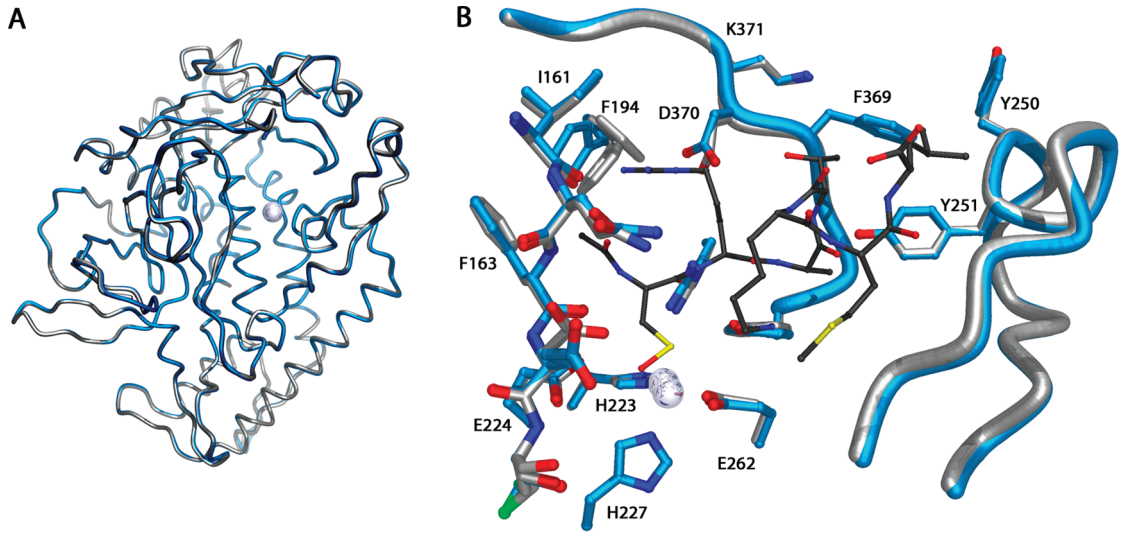

FIGURE 2: Least-squares fitting of the uncomplexed LC (gray) and LC•CRATKML (blue) structures indicates that peptide binding does not induce significant changes in the overall structure of the LC (A) or in the active site (B). Both images were created with POVScript+ (*60*) and POV-Ray.

protease reaction. Thus, it is reasonable to propose that when SNAP-25 binds to the LC, the carbonyl oxygen of the scissile peptide bond selectively displaces W^{Tyr}, positioning the carbonyl carbon for nucleophilic attack by W^{Cat} (Figure 1A). Notably, W^{Tyr} and W^{Cat} are both present in the apo-LC structure, indicating that the active site residues alone are sufficient for proper positioning of the catalytically important groups. This is consistent with a purely catalytic role for the Zn(II) ion (*46, 47*).

Peptide Binding in the BoNT/A-LC Active Site. The structure of LC[425] in complex with the heptapeptide inhibitor *N*-acetyl-CRATKML (LC•CRATKML) was determined to 1.4 Å resolution. Comparison of the LC•CRATKML complex structure with the 1.2 Å-resolution structures of the apoenzyme and the Zn(II)-bound uncomplexed form of the enzyme reveals that binding of the N-Ac-CRATKML peptide does not induce significant changes in the overall structure of the protein (0.5 Å RSMD for all atoms; Figure 2). The first four residues of the heptapeptide, N-Ac-L-Cys, L-Arg, L-Ala, and L-Thr, were all clearly visible in the $|F_o| - |F_c|$ electron density (Figure 3A), even in the earliest stages of refinement. The electron density for the last three residues (L-Lys, L-Met, and L-Leu) was less well defined; therefore, these were added to the model in the later stages of refinement (final B-factors of these residues are 28.6, 31.4, and 44.4 $Å^2$, respectively).

The peptide is bound in the active-site cleft with the Sγ atom of CysP1 positioned 2.3 Å from the catalytic Zn(II) ion (Figure 3B; peptidic inhibitor residues named throughout by three-letter code and Schechter and Berger convention). A strong ($\sim 3.5\sigma$) peak in the $|F_o| - |F_c|$ difference map centered 1.7 Å from CysP1 Sγ and 2.3 Å from the Zn(II) ion persisted throughout the refinement process (Figure 4A and B). Given the proximity of this peak in the difference map to that of the cysteine sulfur, it was originally modeled (after refinement of the protein and solvent model was complete) as a partial-occupancy water molecule (Figure 4C). However, the peptide and the putative water molecule each refined with an occupancy of ~80%. Together, the high occupancy of the putative water and the short distance (1.7 Å) from cysteine Sγ suggest that the atom responsible for the peak in the difference map is covalently bound to the Sγ atom. Modeling the cysteine as cysteine sulfenic acid (S-OH) provided a more satisfactory explanation of the experimental electron density (Figure 4D), eliminating the difference map peak centered near CysP1 Sγ.

The observation of the sulfenic acid raises two questions. First, is the CysP1 Sγ atom oxidized in solution or at the active site? Several observations suggest that the latter is the case. Cysteine sulfenic acid is an unstable intermediate on the paths to sulfinic and sulfonic acids or disulfide bonds (*48*). Stable cysteine sulfenic acid groups are involved in the regulation or catalytic mechanism of several classes of proteins (*49–51*) including matrix metalloproteases (*52*). Thus, if CysP1 were oxidized in solution one would not expect to observe the reactive sulfenic acid in the crystal structure, but if it is formed on the enzyme, the LC may stabilize it. To determine if a significant amount of the sulfenic acid form of the peptide exists in solution, a solution containing 20 mM N-Ac-CRATKML was assayed by MALDI-TOF mass spectrometry (Dana Farber Molecular Biology Core Facility, Boston, MA). The MALDI-TOF spectra of N-Ac-CRATKML were difficult to interpret because of oxidation of MetP6. To address this situation N-Ac-CRATK-Norleucine-L was synthesized and analyzed by MALDI-TOF. The spectra of the norleucine-containing peptide were dominated by a peak consistent in mass with the reduced peptide and showed no peaks having a mass consistent with the sulfenic acid [*m/z*: 826.37, 846.38, 847.38, 848.38, 849.38, 868.36, 884.33, 991.42, 1035.41, and 1058.37], suggesting that this species does not accumulate in solution. To rule out any effect of $Zn(NO_3)_2$ on sulfenic acid formation, N-Ac-CRATK-Norleucine-L peptide (2 mM in H_2O) was incubated for 24 h at 22 °C in the presence of 5 mM $Zn(NO_3)_2$. These conditions replicate those of the crystallographic experiment, except for the omission of the crystallization buffer components (20% PEG 3350 and 0.2 M diammonium tartrate at pH 6.6), which would interfere with mass spectrometric analysis. The $Zn(NO_3)_2$-treated peptide was analyzed by MALDI-TOF, and as before, there was no significant accumulation of the sulfenic acid form of the peptide. Indeed, there was very little oxidation of the

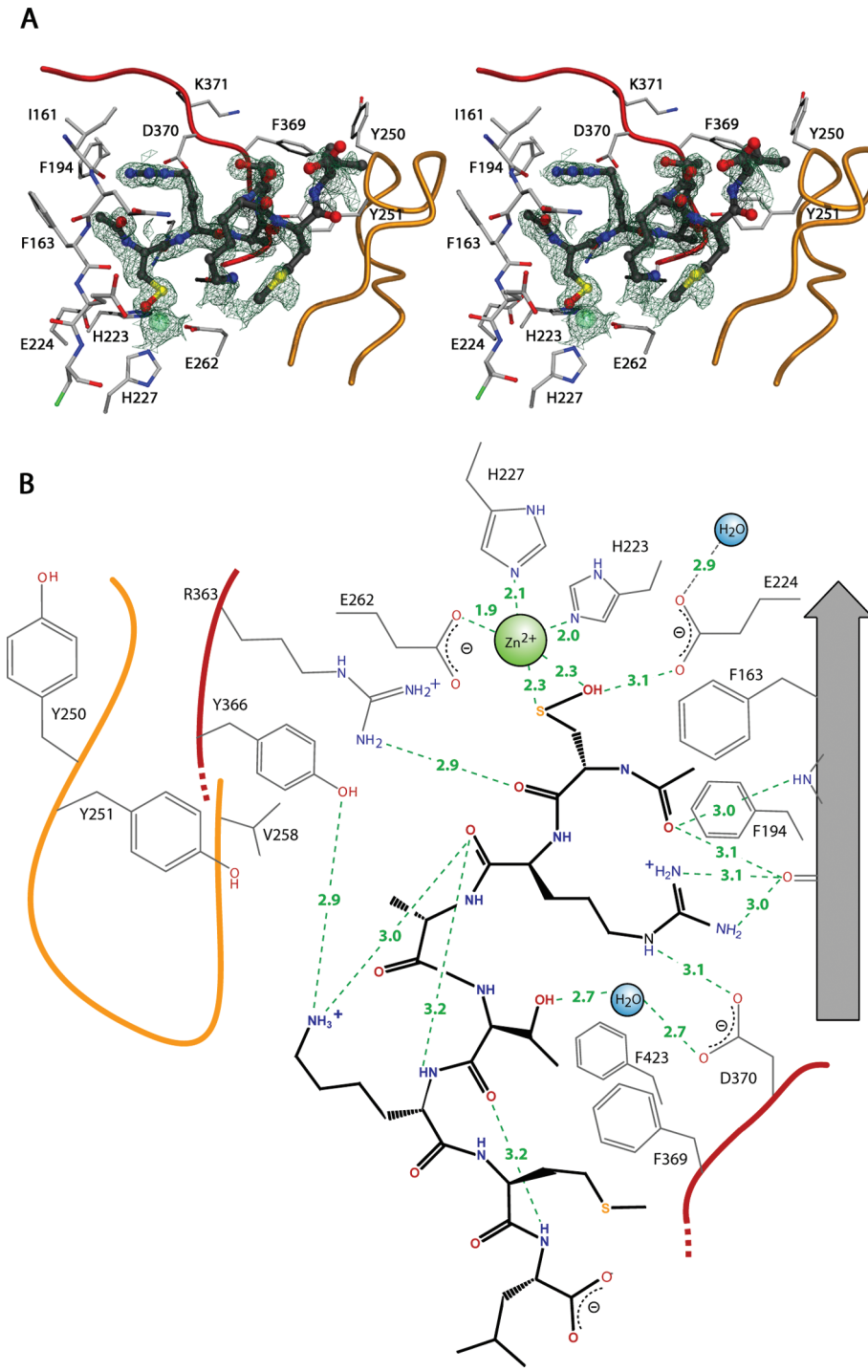

FIGURE 3: Stereo view showing the electron density for the N-Ac-CRATKML heptapeptide (A). The inhibitor is shown in ball-and-stick representation. The electron density (blue mesh) is a $2|F_o| - |F_c|$ composite omit map contoured at 1.1σ. This image was created using MAPMAN (*61*), POVScript+ (*60*), and POV-Ray. Schematic representation of the active site in the LC•CRATKML structure (B) showing the interactions between the peptide and the enzyme. Active site residues are colored gray with thin bonds, and the inhibitor is shown in black with thick bonds. Interactions between the inhibitor and the enzyme active site (hydrogen bonds and van der Waals interactions) are represented by dashed green lines, with distances labeled. The 250 and 370 loops are shown as thick orange and red lines, respectively. Image created with ChemDraw Ultra (CambridgeSoft, Inc.) and Adobe Illustrator (Adobe, Inc.).

CysP1 Sγ atom. The K_i of the norleucine-containing peptide did not differ significantly (within ~2.5-fold) from that of N-Ac-CRATKML (unpublished data), suggesting that the oxidized peptide in solution is not the inhibitory species. In the LC•CRATKML complex structure, one can envision the peptide binding to the enzyme in the reduced form with CysP1 Sγ bound to the Zn(II) ion with W^{Cat} 1.7−2.5Å away. Given this arrangement, and the observation that Zn-bound thiolates are significantly more nucleophilic than Zn-bound alkoxides (*53*), it seems likely that the nucleophilic Sγ atom of CysP1 would then attack the nearby W^{Cat} to form the sulfenic acid. Thus, the oxygen atom observed in the cysteine sulfenic acid might have originated from the catalytic water molecule. Since the resultant peptide is held tightly by the enzyme and there exist no other water molecules nearby, the reactive sulfenic acid is observed bound to the catalytic

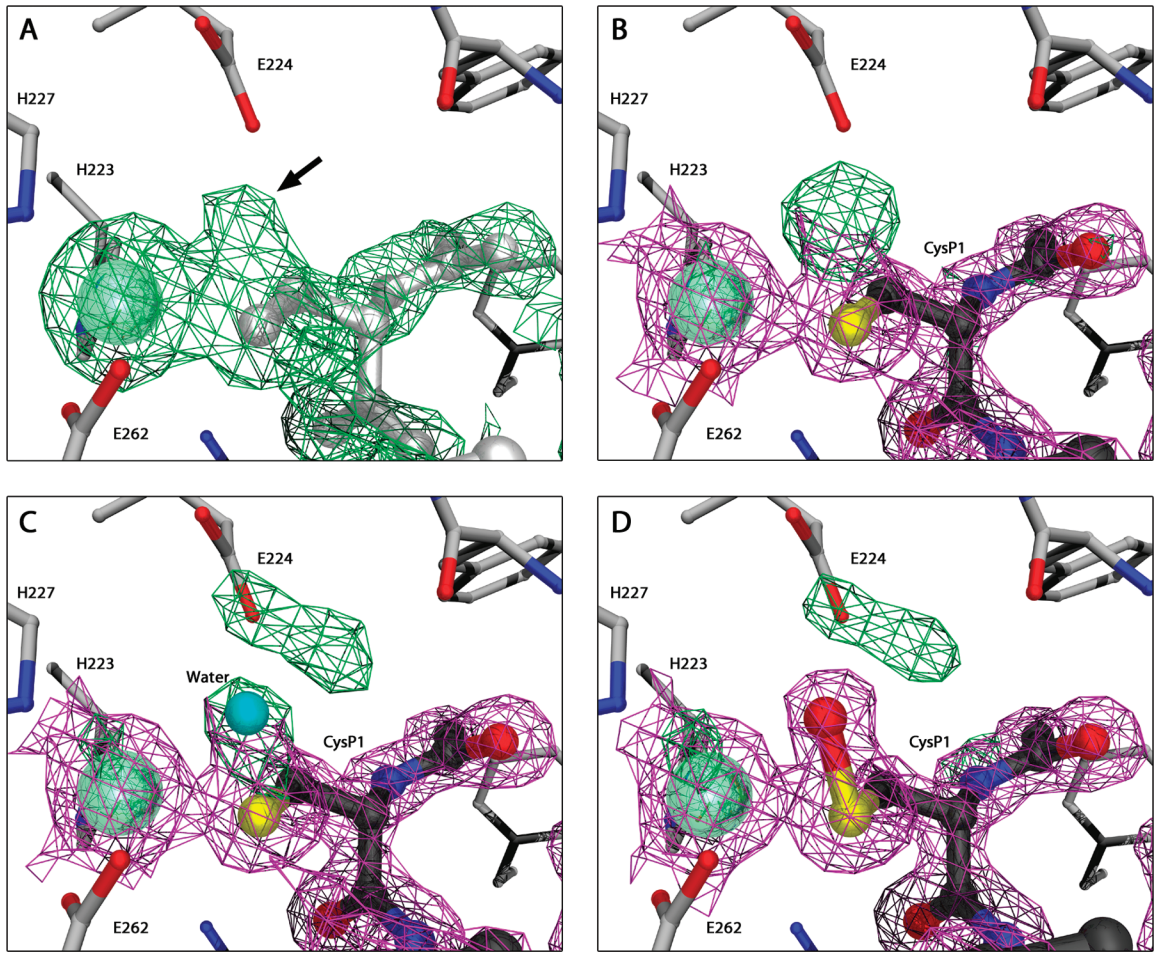

FIGURE 4: Close-up views showing the experimental electron density at the LC•CRATKML catalytic center at various stages of refinement. The catalytic Zn(II) ion is shown as a large, green sphere. Active site residues are shown with gray carbons, and the N-Ac-CRATKML peptide is shown with black carbons. The $2|F_o| - |F_c|$ electron density maps (contoured at 1.5σ) are drawn in magenta wireframe, and the $|F_o| - |F_c|$ difference maps (contoured at 3.0σ) are drawn in green wireframe. Before the N-Ac-CRATKML peptide was modeled (A), there was clear difference electron density that would not be explained fully by CysP1 (arrow). The peptide is included for reference (white metallic ball and stick). After the peptide was modeled (B), a sizable difference peak remained near CysP1 Sγ. Addition of a partial occupancy water molecule (C; cyan sphere) did not account for the difference peak (note the green difference peak remaining near the partial occupancy water molecule). Finally, modeling CysP1 as cysteine sulfenic acid (D) eliminated all difference electron density near CysP1 Sγ. The source of the oblong difference map peak near Glu224 in C and D is unclear. It is not connected to the peak near CysP1 Sγ even at a very low contour level (2.0 σ), indicating that it is not due to a covalent modification of CysP1. All images were rendered using MAPMAN, POVScript+, and POV-Ray.

Zn(II) ion rather than one of the other oxidation products. The enzyme active site is, in effect, protecting the sulfenic acid form of the peptide and not selectively binding the oxidized peptide from solution.

The second question relates to the Zn(II) coordination sphere in the LC•CRATKML complex: what is the coordination geometry, and which atom(s), CysP1 Sγ or Oδ, provide ligands to the Zn(II) ion? Unlike the unliganded enzyme, the Zn(II) ion in the N-Ac-CRATKML complex appears to have distorted-tetrahedral coordination (Figure 1C). Since Sγ and Oδ are equidistant from the Zn(II) ion and both would give distorted tetrahedral coordination geometry (Figure 1C), it is difficult to discern, on the basis of the structure alone, which atom provides the fourth ligand to the zinc. However, the ligand from Sγ results in a less distorted tetrahedron with a Cα-Cβ-Sγ-Zn(II) torsion angle of $-166°$, in good agreement with values observed for similar complexes (*54*). Thus, coordination by Sγ is probably preferred.

The peptide backbone of the inhibitor extends toward the β-exosite with the C-terminus of the peptide lying near the 250 loop. Figure 3B provides the hydrogen-bond lengths and distances for hydrophobic interactions in the active site of the LC•CRATKML structure. The N-terminal acetyl group occupies part of the S1′ subsite identified in structures of the LC in complexes with L-arginine hydroxamate (*39, 44*), making hydrophobic interactions with the phenyl ring of Phe194 and the γ-methyl group of Thr220. The carbonyl oxygen of CysP1 forms a hydrogen bond with Arg363, a residue proposed to stabilize the tetrahedral intermediate formed during catalysis (*55*).

Notably, while ArgP1′ occupies the S1′ subsite, it does so in an unexpected way. Instead of the extended conformation observed in crystal structures with L-arginine hydroxamate (*39, 44*) where the guanidinium group forms a salt bridge with Asp370, the guanidinium group in the LC•CRATKML structure forms a bidentate interaction with the carbonyl oxygen of Ile161, a cation$-\pi$ interaction with

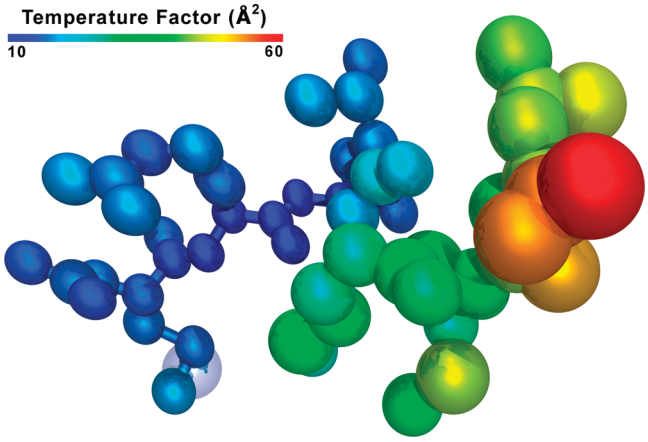

FIGURE 5: Ortep representation of the N-Ac-CRATKML peptide. The size and shape of the atoms indicate the magnitude and direction, respectively, of the atomic motions in the inhibitor. For clarity, the atoms are also colored according to temperature factor with dark blue and red corresponding to B factors of 10 and 60 Å^2, respectively. Image was rendered with POVScript+ (*60*) and POV-Ray version 3.6.1.

Phe194, and a hydrogen bond with the carboxylate group of Asp370. The altered placement of ArgP1′ within the S1′ subsite relative to the L-arginine hydroxamate-bound structures is due to the fact that coordination of the catalytic Zn(II) ion by CysP1 Sγ forces the main chain of the peptide away from the catalytic center toward the 370 loop. Thus, the ArgP1′ side chain does not have sufficient space to form the salt bridge with Asp370 observed in complexes of the LC with L-arginine hydroxamate (*39, 44*). The implications of this observation are clear: the binding mode of the N-Ac-CRATKML peptide is not entirely like that of the true substrate, which would presumably bind with the scissile peptide bond closer to the catalytic center. Therefore, it is evident that inhibitors need not necessarily mimic the natural substrate, for there exist in the active site sufficient opportunities for specific alternate interactions with the enzyme.

The side-chain methyl group of AlaP2′ occupies a hydrophobic pocket formed by Tyr251, Val258, Tyr366, and Leu367. Similarly, the ThrP3′ methyl is bound in a pocket composed of Leu256, Phe369, and Phe423. The Oγ atom of ThrP3′ interacts through a bridging water molecule with Asp370. The ammonium group of LysP4′ forms a hydrogen bond with the hydroxyl oxygen of Tyr366, another active site residue with a catalytic role (*55*) in stabilizing the tetrahedral intermediate. The LysP4′ Nζ also displaces an ordered water molecule observed in the two high-resolution unliganded LC structures. LysP4′ and LeuP6′ make intramolecular interactions (Figure 3B) that cause the peptide to adopt a pro-helical conformation (Figure 3A). MetP5′ does not make any direct contacts with the enzyme, though Cβ packs ~4.0 Å from a side-chain methyl group of Val256. The side chain of MetP5′ interacts more closely with the aliphatic portion of LysP4′ and may be important for positioning the ammonium group to interact with Tyr366. Finally, LeuP6′ makes no direct interactions with the enzyme, a fact that is reflected in the higher temperature factors (Figure 5) and less well-defined electron density (Figure 3A) of this residue.

Insights into Peptide Binding and the BoNT/A-LC Catalytic Mechanism. Together, the structure of the LC•CRATKML complex and the apo and cofactor liganded structures explain earlier kinetic data and shed light on several details of the catalytic mechanism of the BoNT/A-LC. Previous work by Schmidt and Stafford (*36*), and Burnett et al. (*43*) investigated the impact of each residue from P1′ through P6′ on the affinity of the N-Ac-CRATKML-derived inhibitory peptide 2-mercapto-3-phenylpropionyl-RATKML (mpp-RATKML). Their findings indicate that P1′ through P4′ are crucial to binding affinity. In peptides truncated before LysP4′, K_i increases 100- to 200-fold, as might be expected given the loss of the observed favorable hydrogen-bond interaction with Tyr366. Consistent with their relatively high temperature factors, removal of the P5′ methionine resulted in a more modest (10-fold) increase in K_i. Loss of the P6′ leucine or the addition of the last three residues of SNAP-25 (GSG) to the C-terminus of mpp-RATKML had no effect on K_i. Furthermore, sequence modification of each residue showed that, in terms of activity, the only critical side chains are ArgP1′ (>1000-fold increase in K_i for mpp-KATKML), and to a lesser extent, LysP4′ (10-fold increase in K_i for mpp-RATAML) and AlaP2′ (7-fold increase in K_i for mpp-RVTKML). These kinetic data can be explained based on the LC•CRATKML crystal structure.

The failure of Lys to replace Arg in inhibitory peptides is conceptualized by manual modeling of the ArgP1′Lys mutation based on the crystal structure of the complex. The model reveals that the lysine side chain cannot occupy the S1′ subsite in the same manner as arginine. When lysine is positioned to bring the ammonium nitrogen within hydrogen-bonding distance of the Ile161 carbonyl (~2.8 Å), it clashes sterically with Asp370, and the positively charged ammonium group is then no longer in position to form a cation−π interaction with Phe194. There is no conformation of the lysine side chain that allows salt bridge formation with Asp370. Mutation of LysP4′ to alanine removes the hydrogen bond with Tyr366. Furthermore, the lysine ammonium group in the N-Ac-CRATKML complex displaces an ordered solvent molecule. The resultant increase in entropy is likely to contribute significantly to the binding of the N-Ac-CRATKML peptide. Thus, not only would the XKATKML peptide lose a hydrogen bond compared to CRATKML, it would also not benefit energetically from the gain in entropy due to the displaced water molecule.

Formation of unfavorable close contacts explains the results of the AlaP2′Val peptide. When this mutation is modeled, the additional methyl groups clash with Tyr366, Tyr251, Leu256, and Val258. Given the constricted space surrounding the AlaP2′ methyl group, it is surprising that K_i increases by only 7-fold.

It is generally accepted that the conserved Arg363 and Tyr366 residues are responsible for stabilizing the oxyanion that forms in the tetrahedral intermediate of the hydrolysis reaction. The uncomplexed LC structure is consistent with this model. In this structure, there are two water molecules bound to the Zn(II) ion. One is the catalytic water (W^{Cat}) held in place by Glu224 of the HEXXH motif present in many Zn(II) proteases, while the other is bound to Tyr366 (W^{Tyr}). Presumably, when the peptide substrate binds to the enzyme, the carbonyl oxygen of the scissile peptide bond displaces W^{Tyr}. The carbonyl oxygen would then be bound by Tyr366 Oη and Arg363 through a bridging water molecule. These interactions, together with the polarization

of the carbonyl bond by the Zn(II) ion promote the attack of the activated water molecule on the carbonyl carbon.

This structure may explain, at least in part, a curious observation by Breidenbach and co-workers (*20*). In working to obtain the structure of the BoNT/A-LC with the substrate SNAP-25 bound, Breidenbach first mutated Glu224 to glutamine, a residue that would not be competent to act as general base to activate the catalytic water molecule. However, over the time course of the crystallographic experiment, there was significant residual activity. This residual activity necessitated a second mutation, Tyr366 to phenylalanine. The resulting E224Q/Y366F double mutant was completely inactive. There are two possible explanations for the observed residual activity in the E224Q mutant LC and why removing Tyr366 abrogated this activity. The first is that in the E224Q mutant a hydroxide ion from the active-site solvent (although extremely low in concentration) is able to attack the scissile peptide bond, and Tyr366 would then stabilize the intermediate. Since activation of the hydrolytic water is presumably rate limiting in the E224Q mutant LC, if a hydroxide ion occupies the position normally assumed by the catalytic water molecule, the rest of the reaction should proceed normally. Removal of the tyrosine hydroxyl group leaves only the through-solvent interaction with Arg363, which may not be sufficient to stabilize the tetrahedral intermediate. The other possibility is that the phenolate of Tyr366 acts as general base, activating W^{Tyr} to become the catalytic water molecule. The former explanation is the most likely, given the depressed pK_a values observed for Zn(II)-bound water molecules (*56, 57*). Unfortunately, the solvent structure near the catalytic center in the E224Q/Y366F double mutant is unknown since, in the crystal structure (pdb accession code 1XTF (*20*)), the C-terminal His_6-tag binds in the active site, displacing water molecules normally bound to the Zn(II) ion.

Implications for Inhibitor Design. All three of the structures described herein were determined at a higher resolution than any BoNT/A-LC structure available at the time of this writing. The increased resolution provides a more detailed and accurate picture of the solvent structure in the BoNT/A-LC active site. This is significant, given the importance of structural water molecules to the drug-design process. It is not unreasonable to expect a 100-fold decrease in K_i upon displacing an ordered solvent molecule from an enzyme active site (*44*). In addition, the highly accurate atomic positions (estimated standard deviations for all three structures are ~0.1 Å) and the three different states of the active site will inform computational modeling studies and *in silico* screening of inhibitors.

Analysis of the LC·CRATKML structure shows that the N-acetyl group is bound at the entrance to a sizable hydrophobic pocket consisting of residues Phe194, Phe163, Thr220 Cγ, and Thr215 Cγ. With some rearrangement of Phe194, which is known to have considerable mobility (*39*), this pocket should accommodate a phenyl ring or similar hydrophobic group. In addition, the pocket holds two ordered water molecules (present in all three structures) that would be displaced upon binding of a hydrophobic moiety.

Conclusions. The structure of the BoNT/A-LC with the heptapeptide inhibitor N-Ac-CRATKML bound provides the first view of an inhibitory peptide bound in the active site of this enzyme, identifying the structural determinants of specificity. Until now, there has been little structural information available on the binding mode of peptides at the catalytic center. These data, together with the high-resolution unliganded apo- and holo-enzyme structures, improve our understanding of the catalytic mechanism of the BoNT proteases by unequivocally identifying the residues that stabilize the hemiketal oxygens in the tetrahedral intermediate. Furthermore, the structural work presented here will inform efforts to develop potent, small-molecule inhibitors of these lethal neurotoxins.

ACKNOWLEDGMENT

Data for this study were measured at beamline X12B of the National Synchrotron Light Source.

REFERENCES

1. Hambleton, P. (1992) Clostridium botulinum toxins: a general review of involvement in disease, structure, mode of action and preparation for clinical use. *J. Neurol. 239*, 16–20.
2. Hanson, D. (2004) Botulinum toxin: a bioterrorism weapon. *Emerg. Med. Serv. 33*, 55–59.
3. Josko, D. (2004) Botulin toxin: a weapon in terrorism. *Clin. Lab. Sci. 17*, 30–34.
4. Patocka, J., Splino, M., and Merka, V. (2005) Botulism and bioterrorism: how serious is this problem? *Acta Medica (Hradec Kralove) 48*, 23–28.
5. Wein, L. M., and Liu, Y. (2005) Analyzing a bioterror attack on the food supply: the case of botulinum toxin in milk. *Proc. Natl. Acad. Sci. U.S.A. 102*, 9984–9989.
6. Ansiaux, R., Baudelet, C., Cron, G. O., Segers, J., Dessy, C., Martinive, P., De Wever, J., Verrax, J., Wauthier, V., Beghein, N., Gregoire, V., Buc Calderon, P., Feron, O., and Gallez, B. (2006) Botulinum toxin potentiates cancer radiotherapy and chemotherapy. *Clin. Cancer Res. 12*, 1276–1283.
7. Costa, J., Espirito-Santo, C., Borges, A., Ferreira, J. J., Coelho, M., Moore, P., and Sampaio, C. (2005) Botulinum toxin type A therapy for cervical dystonia. *Cochrane Database Syst. Rev.* CD003633.
8. Klaphajone, J., Kitisomprayoonkul, W., and Sriplakit, S. (2005) Botulinum toxin type A injections for treating neurogenic detrusor overactivity combined with low-compliance bladder in patients with spinal cord lesions. *Arch. Phys. Med. Rehabil. 86*, 2114–2118.
9. Ojala, T., Arokoski, J. P., and Partanen, J. (2006) The effect of small doses of botulinum toxin a on neck-shoulder myofascial pain syndrome: a double-blind, randomized, and controlled crossover trial. *Clin. J. Pain. 22*, 90–96.
10. Turton, K., Chaddock, J. A., and Acharya, K. R. (2002) Botulinum and tetanus neurotoxins: structure, function and therapeutic utility. *Trends Biochem. Sci. 27*, 552–558.
11. Lacy, D. B., and Stevens, R. C. (1999) Sequence homology and structural analysis of the clostridial neurotoxins. *J. Mol. Biol. 291*, 1091–1104.
12. Fischer, A., and Montal, M. (2007) Crucial role of the disulfide bridge between botulinum neurotoxin light and heavy chains in protease translocation across membranes. *J. Biol. Chem. 282*, 29604–29611.
13. Dong, M., Richards, D. A., Goodnough, M. C., Tepp, W. H., Johnson, E. A., and Chapman, E. R. (2003) Synaptotagmins I and II mediate entry of botulinum neurotoxin B into cells. *J. Cell Biol. 162*, 1293–1303.
14. Jayaraman, S., Eswaramoorthy, S., Ahmed, S. A., Smith, L. A., and Swaminathan, S. (2005) N-terminal helix reorients in recombinant C-fragment of Clostridium botulinum type B. *Biochem. Biophys. Res. Commun. 330*, 97–103.
15. Lalli, G., Herreros, J., Osborne, S. L., Montecucco, C., Rossetto, O., and Schiavo, G. (1999) Functional characterisation of tetanus and botulinum neurotoxins binding domains. *J. Cell. Sci. 112* (Pt 16), 2715–2724.
16. Finkelstein, A. (1990) Channels formed in phospholipid bilayer membranes by diphtheria, tetanus, botulinum and anthrax toxin. *J. Physiol. (Paris) 84*, 188–190.

17. Lacy, D. B., and Stevens, R. C. (1997) Recombinant expression and purification of the botulinum neurotoxin type A translocation domain. *Protein. Expression Purif. 11*, 195–200.
18. Lacy, D. B., Tepp, W., Cohen, A. C., DasGupta, B. R., and Stevens, R. C. (1998) Crystal structure of botulinum neurotoxin type A and implications for toxicity. *Nat. Struct. Biol. 5*, 898–902.
19. Morihara, K., Tsuzuki, H., and Oka, T. (1968) Comparison of the specificities of various neutral proteinases from microorganisms. *Arch. Biochem. Biophys. 123*, 572–588.
20. Breidenbach, M. A., and Brunger, A. T. (2004) Substrate recognition strategy for botulinum neurotoxin serotype A. *Nature 432*, 925–929.
21. Schmidt, J. J., and Bostian, K. A. (1997) Endoproteinase activity of type A botulinum neurotoxin: substrate requirements and activation by serum albumin. *J. Protein Chem. 16*, 19–26.
22. Hanson, M. A., and Stevens, R. C. (2000) Cocrystal structure of synaptobrevin-II bound to botulinum neurotoxin type B at 2.0 A resolution. *Nat. Struct. Biol. 7*, 687–692.
23. Breidenbach, M. A., and Brunger, A. T. (2005) New insights into clostridial neurotoxin-SNARE interactions. *Trends Mol. Med. 11*, 377–381.
24. Swaminathan, S., and Eswaramoorthy, S. (2000) Structural analysis of the catalytic and binding sites of *Clostridium botulinum* neurotoxin B. *Nat. Struct. Biol. 7*, 693–699.
25. Brunger, A. T., Breidenbach, M. A., Jin, R., Fischer, A., Santos, J. S., and Montal, M. (2007) Botulinum neurotoxin heavy chain belt as an intramolecular chaperone for the light chain. *PLoS Pathog. 3*, 1191–1194.
26. Burnett, J. C., Schmidt, J. J., Stafford, R. G., Panchal, R. G., Nguyen, T. L., Hermone, A. R., Vennerstrom, J. L., McGrath, C. F., Lane, D. J., Sausville, E. A., Zaharevitz, D. W., Gussio, R., and Bavari, S. (2003) Novel small molecule inhibitors of botulinum neurotoxin A metalloprotease activity. *Biochem. Biophys. Res. Commun. 310*, 84–93.
27. Boldt, G. E., Kennedy, J. P., and Janda, K. D. (2006) Identification of a potent botulinum neurotoxin A protease inhibitor using in situ lead identification chemistry. *Org. Lett. 8*, 1729–1732.
28. Park, J. G., Sill, P. C., Makiyi, E. F., Garcia-Sosa, A. T., Millard, C. B., Schmidt, J. J., and Pang, Y. P. (2006) Serotype-selective, small-molecule inhibitors of the zinc endopeptidase of botulinum neurotoxin serotype A. *Bioorg. Med. Chem. 14*, 395–408.
29. Tang, J., Park, J. G., Millard, C. B., Schmidt, J. J., and Pang, Y. P. (2007) Computer-aided lead optimization: improved small-molecule inhibitor of the zinc endopeptidase of botulinum neurotoxin serotype A. *PLoS ONE 2*, e761.
30. Washbourne, P., Pellizzari, R., Baldini, G., Wilson, M. C., and Montecucco, C. (1997) Botulinum neurotoxin types A and E require the SNARE motif in SNAP-25 for proteolysis. *FEBS Lett. 418*, 1–5.
31. Schmidt, J. J., and Stafford, R. G. (2005) Botulinum neurotoxin serotype F: identification of substrate recognition requirements and development of inhibitors with low nanomolar affinity. *Biochemistry 44*, 4067–4073.
32. Schmidt, J. J., and Bostian, K. A. (1995) Proteolysis of synthetic peptides by type A botulinum neurotoxin. *J Protein Chem 14*, 703–708.
33. Evans, E. R., Sutton, J. M., Gravett, A., and Shone, C. C. (2005) Analysis of the substrate recognition domain determinants of botulinum type B toxin using phage display. *Toxicon 46*, 446–453.
34. Chen, S., and Barbieri, J. T. (2006) Unique substrate recognition by botulinum neurotoxins serotypes A and E. *J. Biol. Chem.*
35. Schmidt, J. J., Stafford, R. G., and Bostian, K. A. (1998) Type A botulinum neurotoxin proteolytic activity: development of competitive inhibitors and implications for substrate specificity at the S1′ binding subsite. *FEBS Lett. 435*, 61–64.
36. Schmidt, J. J., and Stafford, R. G. (2002) A high-affinity competitive inhibitor of type A botulinum neurotoxin protease activity. *FEBS Lett. 532*, 423–426.
37. Otwinowski, Z., and Minor, W. (1997) Processing of X-ray diffraction data collected in oscillation mode. *Methods Enzymol. 276*, 307–326.
38. Collaborative Computational Project (1994) The CCP4 suite: programs for protein crystallography, *Acta Crystallogr., Sect. D 50*, 760−763.
39. Silvaggi, N. R., Boldt, G. E., Hixon, M. S., Kennedy, J. P., Tzipori, S., Janda, K. D., and Allen, K. N. (2007) Structures of Clostridium botulinum Neurotoxin Serotype A Light Chain complexed with small-molecule inhibitors highlight active-site flexibility. *Chem Biol 14*, 533–542.
40. Adams, P. D., Grosse-Kunstleve, R. W., Hung, L. W., Ioerger, T. R., McCoy, A. J., Moriarty, N. W., Read, R. J., Sacchettini, J. C., Sauter, N. K., and Terwilliger, T. C. (2002) PHENIX: building new software for automated crystallographic structure determination. *Acta Crystallogr., Sect. D 58*, 1948–1954.
41. Emsley, P., and Cowtan, K. (2004) Coot: model-building tools for molecular graphics. *Acta Crystallogr., Sect. D 60*, 2126–2132.
42. Davis, I. W., Murray, L. W., Richardson, J. S., and Richardson, D. C. (2004) MOLPROBITY: structure validation and all-atom contact analysis for nucleic acids and their complexes. *Nucleic Acids Res. 32*, W615–619.
43. Burnett, J. C., Ruthel, G., Stegmann, C. M., Panchal, R. G., Nguyen, T. L., Hermone, A. R., Stafford, R. G., Lane, D. J., Kenny, T. A., McGrath, C. F., Wipf, P., Stahl, A. M., Schmidt, J. J., Gussio, R., Brunger, A. T., and Bavari, S. (2007) Inhibition of metalloprotease botulinum serotype A: from a pseudo-peptide binding mode to a small molecule that is active in primary neurons. *J. Biol. Chem. 282*, 5004–5014.
44. Fu, Z., Chen, S., Baldwin, M. R., Boldt, G. E., Crawford, A., Janda, K. D., Barbieri, J. T., and Kim, J. J. (2006) Light chain of botulinum neurotoxin serotype A: structural resolution of a catalytic intermediate. *Biochemistry 45*, 8903–8911.
45. Holland, D. R., Hausrath, A. C., Juers, D., and Matthews, B. W. (1995) Structural analysis of zinc substitutions in the active site of thermolysin. *Protein Sci. 4*, 1955–1965.
46. Simpson, L. L., Maksymowych, A. B., and Hao, S. (2001) The role of zinc binding in the biological activity of botulinum toxin. *J. Biol. Chem. 276*, 27034–27041.
47. Eswaramoorthy, S., Kumaran, D., Keller, J., and Swaminathan, S. (2004) Role of metals in the biological activity of Clostridium botulinum neurotoxins. *Biochemistry 43*, 2209–2216.
48. Claiborne, A., Miller, H., Parsonage, D., and Ross, R. P. (1993) Protein-sulfenic acid stabilization and function in enzyme catalysis and gene regulation. *FASEB J. 7*, 1483–1490.
49. Atmane, N., Dairou, J., Paul, A., Dupret, J.-M., and Rodrigues-Lima, F. (2003) Redox regulation of the human xenobiotic metabolizing enzyme arylamine N-acetyltransferase 1 (NAT1): reversible inactivation by hydrogen peroxide. *J. Biol. Chem. 278*, 35086–35092.
50. Seth, D., and Rudolph, J. (2006) Redox regulation of MAP kinase phosphatase 3. *Biochemistry 45*, 8476–8487.
51. Poole, L. B. (2005) Bacterial defenses against oxidants: mechanistic features of cysteine-based peroxidases and their flavoprotein reductases. *Arch. Biochem. Biophys. 433*, 240–254.
52. Shetty, V., Spellman, D. S., and Neubert, T. A. (2007) Characterization by tandem mass spectrometry of stable cysteine sulfenic acid in a cysteine switch peptide of matrix metalloproteinases. *J. Am. Soc. Mass Spectrom. 18*, 1544–1551.
53. Hoffman, J. T., and Carrano, C. J. (2006) S versus O alkylation and coordination in zinc complexes containing the bulky heteroscorpionate alkoxy ligand bis(3,5-dimethylpyrazol-2-yl) diphenylmethanol. *Inorg. Chim. Acta 359*, 1248–1254.
54. Chakrabarti, P. (1989) Geometry of interaction of metal ions with sulfur-containing ligands in protein structures. *Biochemistry 28*, 6081–6085.
55. Binz, T., Bade, S., Rummel, A., Kollewe, A., and Alves, J. (2002) Arg(362) and Tyr(365) of the botulinum neurotoxin type a light chain are involved in transition state stabilization. *Biochemistry 41*, 1717–1723.
56. Evans, S. A., and Shore, J. D. (1980) The role of zinc-bound water in liver alcohol dehydrogenase catalysis. *J. Biol. Chem. 255*, 1509–1514.
57. Krebs, J. F., and Fierke, C. A. (1993) Determinants of catalytic activity and stability of carbonic anhydrase II as revealed by random mutagenesis. *J. Biol. Chem. 268*, 948–954.
58. Lunin, V. Y., Afonine, P. V., and Urzhumtsev, A. G. (2002) Likelihood-based refinement. I. Irremovable model errors. *Acta Crystallogr. Sect. A 58*, 270–282.
59. Holden, H. M., Tronrud, D. E., Monzingo, A. F., Weaver, L. H., and Matthews, B. W. (1987) Slow- and fast-binding inhibitors of thermolysin display different modes of binding: crystallographic analysis of extended phosphonamidate transition-state analogs. *Biochemistry 26*, 8542–8553.
60. Fenn, T. D., Ringe, D., and Petsko, G. A. (2003) POVScript+: a program for model and data visualization using persistence of vision ray-tracing. *J. Appl. Crystallogr. 36*, 944–947.
61. Kleywegt, G. J., and Jones, T. A. (1999) Software for handling macromolecular envelopes. *Acta Crystallogr., Sect. D 55*, 941–944.

BI8001067